Temperature-Dependent, Nitrogen-Perturbed Line Shape Measurements in the ν 1 + ν 3 Band of Acetylene Using a Diode Laser Referenced to a Frequency Comb

ARTICLE *in* THE JOURNAL OF PHYSICAL CHEMISTRY A · OCTOBER 2013

Impact Factor: 2.69 · DOI: 10.1021/jp408960e · Source: PubMed

7 AUTHORS, INCLUDING:

Gary V. Lopez
Brown University
24 PUBLICATIONS **107** CITATIONS
SEE PROFILE

Gregory E Hall
Brookhaven National Laboratory
127 PUBLICATIONS **2,593** CITATIONS
SEE PROFILE

Trevor Sears
Brookhaven National Laboratory
180 PUBLICATIONS **3,540** CITATIONS
SEE PROFILE

Arlan W Mantz
Connecticut College
150 PUBLICATIONS **1,552** CITATIONS
SEE PROFILE

THE JOURNAL OF PHYSICAL CHEMISTRY A

Article

pubs.acs.org/JPCA

Temperature-Dependent, Nitrogen-Perturbed Line Shape Measurements in the $\nu_1 + \nu_3$ Band of Acetylene Using a Diode Laser Referenced to a Frequency Comb

Matthew J. Cich,[†] Damien Forthomme,[‡] Christopher P. McRaven,[‡] Gary V. Lopez,[†] Gregory E. Hall,[‡] Trevor J. Sears,*[†,‡] and Arlan. W. Mantz[§]

[†]Department of Chemistry, Stony Brook University, Stony Brook, New York 11794, United States

[‡]Chemistry Department, Brookhaven National Lab, Building 555A, P.O Box 5000, Upton, New York 11973, United States

[§]Department of Physics, Astronomy and Geophysics, Connecticut College, 270 Mohegan Avenue, New London, Connecticut 06320, United States

ABSTRACT: The P(11) line of the $\nu_1 + \nu_3$ combination band of C_2H_2 was studied using an extended cavity diode laser locked to a frequency comb. Line shapes were measured for acetylene and nitrogen gas mixtures at a series of temperatures between 125 and 296 K and total pressures up to 1 atm. The data were fit to two speed-dependent line shape models and the results were compared. Line shape parameters were determined by simultaneously fitting data for all temperatures and pressures in a single multispectrum analysis. Earlier pure acetylene measurements [Cich et al. *Appl. Phys. B* **2012**, *109*, 373−38] were incorporated to account for self-perturbation. The resulting parameters reproduce the observed line shapes for the acetylene-nitrogen system over the range of temperatures and pressures studied with average root-mean-square observed-calculated errors of individual line measurement fits of approximately 0.01% of maximum transmission, close to the experimental signal-to-noise ratios. Errors in the pressure measurements constitute the major systematic errors in these measurements, and a statistical method is developed to quantify their effects on the line shape parameters for the present system.

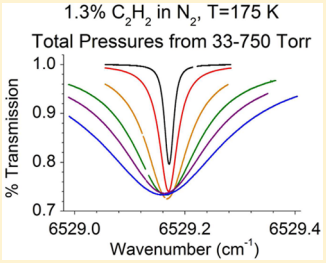

1. INTRODUCTION

The characterization of spectral line shapes is vital to fields as diverse as remote sensing, astronomy, analytical spectroscopy, and the molecular physics of collisions. Improvements in laboratory techniques and measurements provide the empirical data that drive advances in these fields and the relatively strong $\nu_1 + \nu_3$ combination band of acetylene at 1.5 μm has long been used as a model system.[1−3] From a practical standpoint, acetylene in the earth's atmosphere[4,5] has been linked to industrial processes[6] and marine sources,[7] and may even have influenced the evolution of the earliest organisms.[8] Elsewhere in the solar system, acetylene in Titan's atmosphere[9] contributes to a complex photochemistry involving hydrocarbons[10] and the study of this chemistry has been of much recent interest as a model for the atmosphere of proto-earth type planets.

Spectroscopic measurements of the $\nu_1 + \nu_3$ band of acetylene are numerous, and following the first frequency-based optical measurements,[11] the isolated rotational lines have been used as secondary frequency standards.[12] They were also some of the earliest molecular spectra measured referenced to a frequency comb[13,14] in 2005.[15,16] Line shape parameters for this band have been determined for pure acetylene and for acetylene in collisions with nitrogen and inert gases[2,17−20] and others listed in ref 21. Several recent studies have measured the temperature dependence of collisionally perturbed line shapes for both self-collisions[22] and collisions with N_2.[18,19] The first line shape measurements to take advantage of the precision and accuracy of frequency comb-referenced techniques, such as those mentioned in a review by Margolis,[23] were made on the P(11) line of this band. The frequency accuracy of the external cavity diode laser (ECDL) used as the light source in these measurements was shown[24] to be 2.5 parts in 10^{12}. More recently, CO_2[25] and CH_4[26] line shape measurements have also been made using frequency comb-referenced techniques.

In the present work, we have studied the effects of nitrogen collisions on the acetylene absorption line shape for the P(11) line in the $\nu_1 + \nu_3$ band of acetylene at pressures of up to 1 atm and at a series of temperatures between 125 and 296 K. In our previous work[22] it was found that acetylene line shape measurements over a wide range of conditions were best reproduced using a speed-dependent Voigt (SDV)[27] line shape model. In that work, other line shape models, including Voigt,[28] Rautian,[29,30] Galatry[31] and RGP[32] were tested, but could not reproduce the observations as well as the SDV. In this present work we have used two closely related SDV models, which will be described in detail below. The models reproduce the new nitrogen-broadened data with similar accuracy to that found previously for the self-broadened measurements.

Special Issue: Terry A. Miller Festschrift

Received: September 6, 2013
Revised: October 12, 2013
Published: October 14, 2013

In contrast to the previous work, we have analyzed data for all temperatures and pressures together in a single multispectrum fit. Fitting all the temperatures and pressures together ensures that the derived parameters, in particular those with well-characterized temperature-dependent behavior, are consistent across the entire range of experimental conditions.[33] This was not possible in the earlier work when data at each temperature were treated separately by the fitting program used. The new procedure became practicable due to the development of more efficient computer codes to analyze the data. Depending on which model was used, the final nitrogen-perturbed line shape data are described by very few parameters described in section 3.1. For the first time, the temperature dependence of difficult-to-measure speed dependence parameters associated with the narrowing and asymmetry of the line are reported. The earlier self-broadened data were included in the analysis, and the resulting fit parameters can be used to model line shapes for acetylene-nitrogen mixtures over the full range of naturally occurring concentrations, pressures, and temperatures using the extended multispectrum analysis. In the present work, unlike previously,[22,24] an attempt has been made to estimate parameter uncertainties accounting for systematic pressure measurement uncertainties. These become an important factor in determining true parameter uncertainties when other sources of error, such as in the frequency measurement, are small.

2. EXPERIMENTAL METHODS

The experimental setup was similar to that used previously.[22,24] Briefly, a Menlo Systems FC-1500 Optical Frequency Synthesizer based on a mode-locked erbium fiber laser with a broadened output extending from 1050 to 2100 nm was used to stabilize the output of a 1550 nm ECDL (Sacher TEC 520 with Sacher Pilot PC controller). A sample of the ECDL output was offset-locked to a single comb line. The remaining diode laser power was used as the spectroscopic source. In order to scan the ECDL, the comb repetition rate was changed stepwise on the order of a few hertz, corresponding to an optical frequency change of several hundred kilohertz. Previously the repetition rate was changed by 4 Hz per step, corresponding to a 783 kHz step of the ECDL. For the most recent data (about 1/3 of the current data set), the number of data points was reduced by using 16 Hz repetition rate steps between each acquisition point. A fast series of micro steps were made between each data point to maintain the comb-laser lock, and improved software checked for system stability before beginning the acquisition at each point. A telescope in the beam of the ECDL probe was added to reduce the beam divergence and improve the transmission through the narrow aperture optics such as an electro-optic modulator. These changes led to reduced analysis time by reducing the number of data points, and significantly improving the overall data quality.

The sample was held in a temperature controlled copper cell.[24,34] For the current experiments, measurements in samples with low acetylene concentrations, i.e., from 0.01% to 2.5% were taken using a 16.551 cm (measurements are at 296 K) cell. A shorter 1.085 cm cell was used for measurements at high (25% or 50%) acetylene concentrations, which were later omitted from the analysis as described later. Length measurements were made with a precision micrometer with estimated errors of ±0.0005 cm. Data were recorded in transmittance mode in a dual beam setup. A single optical scan could be up to 2.5 GHz long, limited by the available servo-lock voltage controlling the comb laser cavity length. Broader line profiles were recorded by concatenating successive overlapping scans containing line segments as before.[24] Some examples are shown in Figure 1.

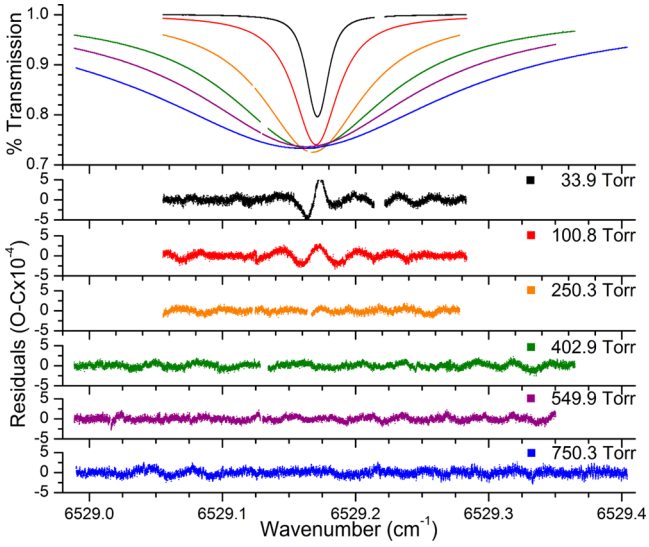

Figure 1. Example spectra taken at a concentration of 1.3% C_2H_2 in N_2 at 175 K. Overlaid in the top plot are the raw experimental data. The lower panels contain expanded residuals of the observed-minus-calculated data points at 6 different pressures, obtained with the SDV model. Due to instrumental constraints, broader line shapes needed to be taken in several segments and were later concatenated, leaving small gaps where no data exists.

The temperature was recorded at each frequency step with an accuracy of between 0.125 and 0.105 K, and precision of 0.0001 K.[22] Pure acetylene gas (>99.6%, MG gases) was used, and the residual acetone was removed by passage through a cold trap maintained at 178 K prior to use. Several samples were checked by mass spectrometry to ensure purity. Nitrogen-gas (Matheson, extra dry) was used without further purification. An MKS model 690A013TRA 0−1000 Torr Baratron capacitance manometer gauge head, with certified accuracy of better than 0.04% across the entire range, was used for pressure measurements. However, zero offset drifts of up to 0.5 Torr were noted over periods of days during which the data were collected. A small part of the current data set was recorded using an older gauge (MKS 310BHS 1000 Torr). These data were corrected based on calibrations using the new gauge resulting in an estimated accuracy of 0.5% for these measurements. The pressure was monitored and recorded at each step of data acquisition, and varied by no more than the quoted accuracy during a scan of duration 25 min. Line profiles were typically recorded using a high-pressure sample of nitrogen containing a low concentration of acetylene at a given temperature and repeated at successively lower pressure as fractions were pumped out, maintaining the original concentration. Pressure gauge zero drifts over the periods data were recorded constitute the major systematic errors in the measurements and affect the lower pressure line shapes more acutely.

It was necessary to include the earlier pure acetylene broadening measurements to account for the small partial pressure of acetylene present in current measurements, as described in section 3. The vapor pressure of acetylene[35]

dx.doi.org/10.1021/jp408960e | J. Phys. Chem. A 2013, 117, 13908−13918

limited measurements to minimum temperatures of 150 and 125 K for pure C_2H_2 and N_2-broadened samples, respectively. At 125 K the vapor pressure of acetylene is only 0.4 Torr. For pure C_2H_2 a total of 67 line measurements were made in a total of 152 segments. Pressures ranged between 3 and 350 Torr. The N_2-broadened C_2H_2 data set includes 62 line measurements made in a total of 199 segments. Concentrations between 3% and 0.3% were included in the final fit data set. Some additional details are given in section 4.1. Total mixture pressures ranged from 5 to 750 Torr.

3. THEORETICAL METHODS

3.1. Line Shape Model. A satisfactory line shape model needs to be able to account for observed line shapes over the entire range of temperatures, pressures, and concentrations. In the high pressure limit, many standard line shape models perform well as they correctly predict a limiting Lorentzian profile. At pressures lower than those included in the present data, pressure broadening is negligible, and a Gaussian profile corresponding to Doppler broadening is observed for gases in a near collision-free environment. However, line profiles at intermediate pressures can be difficult to predict, and the choice of line shape model is important. Here the effects of collisions on the observed line shape depend on various intermolecular interactions that have been modeled using a number of different assumptions and derived parameters. For a model to be useful for extracting species concentration data from remote sensing measurements, these interactions need to be described with parameters that scale in a well-defined way with changing pressures and temperatures.

The simplest such model is the Voigt profile,[28] a convolution of Gaussian and Lorentzian line shapes. Temperature-dependent Lorentz broadening ($\gamma(T)$) and a collision-induced line shift ($\delta(T)$) parameters are those typically used in the Voigt model. The Voigt profile has well-known deficiencies due to its neglect of collisional narrowing that is commonly observed at low to intermediate pressures[36] resulting in erroneously small estimates for $\gamma(T)$. More sophisticated line shape models, such as the hard-collision (Rautian-Sobel'man[29,30]), soft-collision (Galatry[31]), and hybrid hard/soft-(RGP) collision profiles include a confinement narrowing parameter ($\gamma_{\mathrm{Dicke}}(T)$) and result in larger $\gamma(T)$ values. These models perform much better than the Voigt profile for line shapes recorded at intermediate pressures. However, for low-temperature, higher density measurements in particular, clear asymmetries in the line profiles, often interpreted as being the result of speed-dependent collision effects[37] on the shift, $\delta(T)$, can be observed. Asymmetry has also been reported in measured line profiles of water[38] and acetylene[39] as well as in our earlier work.[22] Aside from the effect of speed dependence on the shift, correlations between velocity-changing and phase-changing collisions in the context of a Dicke narrowing model can also result in asymmetry,[40] and a separation of the effects of these possible mechanisms has been a focus of several recent studies.[39,41,42]

We previously found,[22] that of the tested models (i.e., Voigt, SDV, hard and soft collision), the SDV model[27] best fit the experimental data over the entire temperature and pressure range for acetylene self-broadening. This line shape model, taken directly from Ward et al.,[27] includes the velocity- and impact parameter-averaged semi-classical speed-dependent phase shifts induced by an isotropic, inverse power law, V, $V \propto r^{-q}$, approximated by an inverse power, q, of the intermolecular distance, r, and assuming straight line trajectories. The temperature- and pressure- independent parameter, q, accounts for both speed-dependent narrowing and asymmetry in the line shape. For many physical models of the intermolecular potential, a value of q near 6 is expected, and qualitatively this has been observed.

In the present work, we consider two variants of a speed-dependent line shape model and find that both reproduce the data to close to the experimental noise, i.e., a fractional noise of 1×10^{-4}. Explicit nonlinear line mixing effects[43] are not taken into account since P(11) is effectively isolated at the pressures in this study. The line separation is such that adjacent lines in this band cannot be efficiently coupled by collisional energy transfer at pressures less than ~5 atm. given the measured $\gamma(T)$. The additive effects of the wings of two hot band lines were however included, as detailed below.

For each gas the SDV profile includes the three parameters mentioned above: $\gamma(T)$, $\delta(T)$, and q. The effective intermolecular potential parameter q is assumed to be temperature-independent, but $\gamma(T)$ and $\delta(T)$ are assumed to have a temperature dependence consistent with that used in the HITRAN database:[44]

$$\frac{X(T)}{X(T_0)} = \left(\frac{T_0}{T}\right)^{n_X} \tag{1}$$

where $X(T)$ is either the broadening or shift at a given temperature T (K) for either C_2H_2 or N_2 as perturber, in cm^{-1}/atm, T_0 is the reference temperature (296 K), and n_x is the temperature-dependence exponent to be fit. Several assumed descriptions for temperature dependence of $\delta(T)$ have been used in the past.[45,46] There is a possibility that the shift parameter may pass through zero at certain temperatures for some systems, and a linear (or polynomial) function in the temperature can be used to fit the observations instead.[45] Either model is empirical, but the variation of eq 1 was chosen to model the shift because it resulted in a slightly better fit than a linear model and is consistent with the broadening parameter.

Pressure effects due to collisions among all gases in the mixture need to be taken into account in modeling the observed profiles. The total broadening and shift parameters for any given absorber speed were estimated as the sum of the pressure-weighted contributions of each present molecule, multiplied by a unitless function, $\beta(\nu_a,q)$ adapted from Ward et al.,[27] eq 7.7:

$$\beta(\nu_a, q) = \left(1 + \frac{m_p}{m_a}\right)^{q-3/2q-2} \sum_{n=0}^{N} \frac{\left(\prod_{j=0}^{n-1} -\frac{q-3}{2q-2} + j\right)\left(-\frac{m_p \nu_a^2}{m_a \nu_{a0}^2}\right)}{\left(\prod_{j=0}^{n-1} \frac{3}{2} + j\right) n!} \tag{2}$$

where m_p is the perturber mass, m_a is the absorber mass, ν_a is absorber speed, and ν_{a0} is the most probable absorber speed $(2k_BT/m_a)^{1/2}$. Care must be taken to choose N to be large enough for $\beta(\nu_a,q)$ to converge. In the SDV model, a convolution over all absorber speeds gives the line shape.

The approximations giving rise to q in SDV are not physically realistic, and we find small but real deficiencies in the line shape modeling results, as discussed below. For this reason, we have examined another model,[47−49] parametrized in the time domain, which includes separate empirical parameters for

speed-dependent narrowing and asymmetry and described in detail previously (Forthomme et al.,[50] cf. eqs 2−7]). In principle, this model can incorporate both Dicke and speed-dependent narrowing.[41,51−53] The essential elements are described below. It has been termed the speed-dependent Galatry[47,49,54] model. However, in common with other recent reports,[49,55] due to the strong correlation between parameters representing the two narrowing effects, it has not been possible to allow both to vary in the analysis. We have set the Dicke narrowing parameter (γ_{Dicke}) to zero, hence the name Quadratic Speed-Dependent Voigt (Q-SDV), derived from the quadratic form assumed for the speed dependence of the relaxation rate when averaged over collider velocities. In the Q-SDV model, a phenomenological relaxation rate (in s^{-1}) depending on the pressure- and temperature-dependent parameters (Γ) is given by the form:[48]

$$\Gamma(\nu_a) = \Gamma_0 + \Gamma_2\left[\left(\frac{\nu_a}{\nu_{a0}}\right)^2 - \frac{3}{2}\right] \tag{3}$$

where Γ_0 is the speed-independent portion of the relaxation and Γ_2 is a parameter characterizing the speed-dependence of the complex relaxation rate. The real and imaginary parts of Γ_0 give the broadening and shifting, while real and imaginary parts of Γ_2 give the narrowing and asymmetry according to:

$$\Gamma_0 = 2\pi c[\tilde{\gamma}_{\mathrm{Tot}}(T) - i\tilde{\delta}_{\mathrm{Tot}}(T)] \tag{4}$$

$$\Gamma_2 = 2\pi c[\tilde{\gamma}_{2,\mathrm{Tot}}(T) - i\tilde{\delta}_{2,\mathrm{Tot}}(T)] \tag{5}$$

where each parameter $\tilde{\gamma}_{\mathrm{Tot}}, \tilde{\gamma}_{2,\mathrm{Tot}}, \tilde{\delta}_{\mathrm{Tot}}, \tilde{\delta}_{2,\mathrm{Tot}}$ (in cm^{-1} units) is a sum of contributions from contributing collision partners, weighted by p_i, the partial pressure of component gas i. For example:

$$\tilde{\gamma}_{\mathrm{Tot}}(T) = \sum_{i=\mathrm{gas}} p_i[\gamma(T)]_i \tag{6}$$

where the more commonly used broadening parameter $\gamma(T)$ has units of cm^{-1} atm^{-1}. This model, while not specifically identifying parameters with specific individual physical interactions, does remove restrictions that the SDV model creates because of its direct link between narrowing and asymmetry. Additionally, the four parameters are effective in qualitatively describing observed perturbations to the line shape, and the derived parameter values can be assessed with respect to their physical origin after the fitting, hence removing possibly unphysical model details from the fitting process. Contributions due to individual gases, $\gamma(T)$ and $\delta(T)$, are assumed to follow eq 1 in their temperature dependence. As part of the data analysis in section 4.2, the temperature dependence of $\gamma_2(T)$ and $\delta_2(T)$ will be explored since prior experiments have not investigated the trends.

3.2. Multispectrum Fitting Program/Fitting Procedure. In our previous study employing the SDV model,[22] self-collision data for each temperature were previously analyzed separately, resulting in a value for $\gamma(T)$, $\delta(T)$, and q at each measured temperature. Under these conditions, q varied but showed no well-defined trend with temperature. The temperature exponents n_γ, and n_δ were subsequently determined by fitting the sets of independently determined values of $\gamma(T)$ and $\delta(T)$ to eq 1. A new multispectrum fitting code has been developed, which fits the SDV (or Q-SDV) models and allows for fitting of all the self- (or N_2-) broadened spectra simultaneously. Now only two parameters describing the broadening, $\gamma(T_0)$ and n_γ, were determined, and the power law of eq 1 was used as a constraint on the temperature dependence. For the SDV model, a q in accord with the entire data set was determined. In preliminary fits, the remaining parameters were allowed to float independently at each temperature; this includes $\delta(T)$ for SDV and $\delta(T)$, $\gamma_2(T)$, and $\delta_2(T)$ for Q-SDV. As clear trends were noted that additional temperature-dependent constraints were added as described in section 4.2.

For a satisfactory fit, it is crucial that the line amplitude be correct, yet there are many relatively poorly characterized contributions to it. For example, the line strength values have estimated uncertainties of 2%[56] in the HITRAN 2012 database.[44] The partial pressure of the absorbing gas is subject to the pressure gauge uncertainties, which can be relatively large at low partial pressures. Nonideal gas behavior[57] could contribute as much as 3% to our measured amplitudes, and baseline uncertainties can also be correlated with the amplitude. The line intensity is also subject to any minor path length reductions due to copper contraction as the temperature is reduced. The path length is expected to decrease by about 0.3% from room temperature down to 125 K. These uncertainties combine to create a line amplitude that is approximate and does not properly fit the data. Therefore the overall line amplitude for individual line measurements was allowed to vary in our analysis by incorporating a variable correction factor that is approximately equal to unity. Most sources of uncertainty will be accommodated by this. In principle, the measured line intensity could be used to calculate a new pressure and derive parameters in a fit including the revised pressure. However, trial calculations resulted in a decreased fit quality of close to a factor 10 in the root-mean-square error, and resulted in large systematic residuals, indicating that a simple pressure measurement shift is not the sole contribution to the amplitude errors. If a single pressure and temperature line profile measurement included several segments then a single value for the line amplitude correction was assumed for the full line. Linear effects due to overlapping hot band lines can affect the values and temperature dependence of fitted parameters for the line of interest if not taken into account. The R(9)e of (10111) ← (00011) and the R(11)e of (10120)←(00020) lines were included in the modeling using Voigt parameters fixed at the HITRAN[44] values. Since they are 3 orders of magnitude weaker than the fundamental transition of interest, this effectively removes them as a possible contribution to systematic errors or uncertainty. In all cases, the pure C_2H_2 data were evaluated first with the results being imported into the C_2H_2−N_2 data fitting as fixed values.

4. RESULTS AND DISCUSSION

4.1. Quality of Data. As a measure of fit quality, a root-mean-square error (RMSE), derived from the squared differences between experimental transmission data points and calculated values, was calculated for each line measurement. The average RMSE for pure C_2H_2 line measurements was 0.011% of the maximum transmission for both SDV and Q-SDV models. RMSEs are very similar across the entire data set, with a slight trend of higher RMSEs as pressure and temperature decrease.

The baseline in each data file (representing either a full line or segment) was represented by an adjustable offset, slope, and curvature and is dominated by random uncorrelated drift of the

dx.doi.org/10.1021/jp408960e | J. Phys. Chem. A 2013, 117, 13908−13918

signal in the two detection channels. Attempts were initially made to fit with only an offset and slope, which are necessary due to a drift in the ratio of the signal and reference channels and a wavelength-dependent drift caused by the changing laser diode current in the frequency stabilization locking loop, respectively. With only two baseline parameters the residuals contain small, but clearly observable features attributed to the drift in the signal ratio. Adding the third, quadratic, term to the baseline removes these features from the residuals and results in a factor of 2 improvement in RMSE. Each individual file measurement has a unique baseline that requires individual treatment. This implies that in the broader line shapes requiring multiple segmented scans, there is little useful information in partial segments in which a line center is not present, as the baseline can accommodate a large variety of different parameter values. In the SDV model, parameters were unchanged within their expected uncertainty when adding the quadrature parameter to the baseline (or even from a fit with only a single offset parameter) indicating that the multispectrum fit is not being biased by the additional parameters. However, the additional flexibility in the Q-SDV model causes the inclusion or exclusion of the curvature to change the values for the parameters of interest. Based on the improved RMSE and residual quality, we believe that including the curvature removes most baseline inconsistencies, which may negatively influence parameters that could accommodate the features such as the line asymmetry. Improvements to the spectrometer are in hand to reduce the baseline variation.

The data illustrated in Figure 1 are from a range of pressures at a constant 1.3% concentration and 175 K temperature from the $N_2-C_2H_2$ measurements. The observed−calculated residuals shown are representative of the line shape fits. For the two line profile models compared here, the average RMSE of all the measurements was 0.0095% of the maximum transmission for the SDV and 0.0089% for the Q-SDV. The RMSE was below 0.19% of the peak absorption in any line measurement for either model. While the N_2-broadened line shape fits have, on average, slightly smaller RMSE values than the self-broadened fits, the distribution showed some systematic trends. Lower pressure line shapes tended to have slightly poorer RMSE values, representing a less than perfect fit. Often the baseline variation of a line segment was fit imperfectly, resulting in visible features within the residuals above the spectrometer noise. Data recorded using the new spectrometer software controls described above had smaller than the average RMSE.

The lowest pressure data in Figure 1 show small, but systematic, deviations between the measured and calculated line profiles at line center, characteristic of inaccurate modeling of the narrowing and shifting contribution to the line shape at the nominal recorded pressure. Many of the measurements taken at pressures lower than 100 Torr showed similar discrepancies. We do not believe the problems are due to model deficiencies, since, if removed from the multispectrum fit, each independent line measurement can be fit with much reduced systematic residuals, retaining the global multispectrum line shape parameters, but adjusting only the pressure by a few tenths of a Torr, an error we now attribute to a zero offset drift unrecognized at the time of data acquisition. For example, the error in the 33.9 Torr line profile at 175K in Figure 1 is consistent with a pressure error of less than 1%. Other data (not shown) had residuals representative of similar pressure differences, but with the opposite sign, while still others were flat.

Figure 2 shows sample N_2-broadened data residuals resulting from both line shape models, covering a variety of temperatures

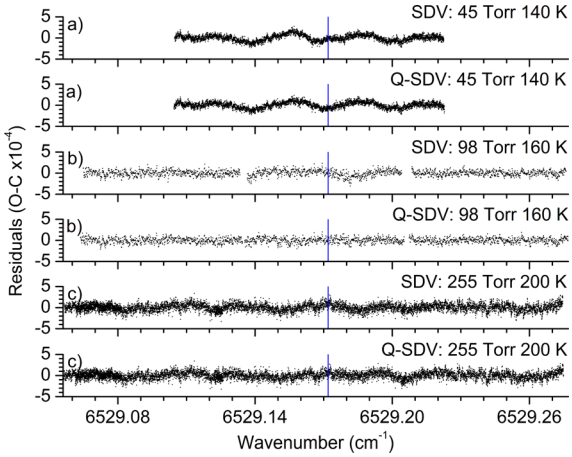

Figure 2. An example comparison of N_2-broadened data residuals (observed−calculated) calculated using SDV and Q-SDV models. A vertical blue line is drawn at line center for reference. (a) 45 Torr and 140 K. (b) 98 Torr and 160 K. (c) 255 Torr and 200 K.

and pressures. At higher pressures, the models give nearly identical fits. As pressure decreases, both models often show inexact modeling of the narrowing, as discussed above, leading to the "w" or "m"-shaped residuals at line center, primarily due to small pressure errors, combined with the constraints of the multispectral fit. Q-SDV fits exhibit slightly smaller and more symmetric residuals at all pressures, presumably a result of the model's additional flexibility.

The effects of systematic errors in pressure are not normally accounted for in line shape analyses, because errors in the frequency measurements are comparable or larger. For the present work, the frequency uncertainty in the data is negligible. Least squares fits to the data that do not include an account of the pressure (or other variable, such as temperature) uncertainty result in derived parameters with artificially small statistical uncertainties.[58] A robust way of including uncertainties in secondary measured quantities uses a Monte Carlo technique described, for example, in Bevington and Robinson.[59] We have implemented a variation of this procedure in order to derive realistic parameter uncertainties. We assume the maximum pressure error in each measurement is at the level of 0.5%. This is a conservative estimate: the true error is likely smaller. For each line measurement, 500 new pressures were computed. They were distributed with a Gaussian probability function about the measured pressure, with a standard deviation of 0.5% of the measurement. The overall fit was then repeated 500 times using the vector of new pressures for each line measurement, generating a distribution of the fitted parameter values. A standard deviation σ_{SDV} (or $\sigma_{Q\text{-}SDV}$) was obtained for each of the parameters by combining the results of all the data set fits (indexed by j):

$$\sigma_{SDV} = \sqrt{\frac{\sum_{j=1}^{N}(X_j - \bar{X})^2}{N-1}} \quad (7)$$

where X_j is a parameter with average over all fits of $\bar{X}$, and N is the number of data sets, 500 here. Five hundred samples resulted in well-converged standard deviations. These standard deviations are reported in Tables 1−4 as the "P-smeared"

Table 1. Self-Broadened Line Shape Parameters for the P(11) Line of $\nu_1 + \nu_3$ Derived from Data in Ref 22

	SDV		Q-SDV		
fitted parameter	value (uncertainty)	P-smeared uncertainty	value (uncertainty)	P-smeared uncertainty	ref 22
$\gamma(T_0)^a$	0.152531(8)	0.0006	0.154788(16)	0.0011	0.149912(8)
n_γ	0.68763(8)	0.007	0.68541(19)	0.01	0.7035(61)
$\delta(T_0)^a$	−0.007885(1)	0.00002	−0.008166(4)	0.00005	−0.007676(2)
n_δ	0.07094(39)	0.005	0.05309(90)	0.01	0.086(10)
q	7.353(3)	0.09	---	---	6.240(5)-7.61(3)^b
$\gamma_2(T_0)^a$	---	---	0.02141(1)	0.0006	---
$n_{\gamma 2}$	---	---	0.657(1)	0.04	---
$\delta_2(T)^a$	---	---	See Table 3	See Table 3	---

^{a}Units are cm^{-1}/atm. Reference temperature T_0 is 296 K. Values are reported with one standard deviation in parentheses. Columns 3 and 5: Uncertainties obtained by assuming a 0.5% pressure uncertainty, and Monte Carlo sampling; see text for details. $^b q$ parameters in ref 22 followed no trend but did change with temperature.

uncertainties. Naturally, these numbers are larger than the statistical estimates derived from the standard fitting procedure, but account for the pressure uncertainties such that the "true" parameters certainly lie within these limits.

Fitted line amplitudes for the pure C_2H_2 SDV data are higher than HITRAN's reported values,[44] and a pressure-dependent trend is noted. At pressures less than 100 Torr, calculated intensities tend to be approximately 2% higher than HITRAN's values. At higher pressures, intensities are no longer consistent; there is as much as an 8% difference from HITRAN, and some measurements were lower than expected, although the great majority were within 4%. This is because the high pressure data are recorded in segments and particularly subject to baseline uncertainties. For the N_2 broadened data, the partial pressure of C_2H_2 is very small, and the amplitude correction factor accommodates this pressure error. The line shape parameters are determined by the much larger N_2 pressure.

Some data were recorded at approximately 25% and 50% acetylene concentrations (160 and 80 Torr total pressure, respectively) at 175, 200, and 240 K. Unlike the pure C_2H_2 or low concentration data, in the high concentration data, the line shapes contain significant contributions due to collisions involving both gases, implying pressure uncertainties will have a greater effect. It was found that the multispectrum fit depended more heavily on the concentrations chosen for these line measurements than for the rest and were ultimately unable to reconcile them with the low concentration data. We have found no literature reports of speed-dependent line shapes being used to model mixtures of gases where one gas is not in low concentration, and for the SDV model, the effective potential exponent, q, is not necessarily expected to follow a simple additive mole faction scaling with concentration. Because of the small number of measurements at high concentration, it was difficult to determine whether the problems encountered are a result of the line shape model used, increased pressure uncertainties, or the treatment of the concentration-dependent effective broadening parameters. In the future, we will obtain a more extensive data set to investigate the cause of the difficulties encountered here.

4.2. SDV Modeling. Table 1 contains the parameters determined from the fits to the self-collision data, with statistical errors of one standard deviation in parentheses. The overall quality of the fit to the observations is similar to before[22] and by extending the multispectrum fitting by using only two broadening parameters for all temperatures in the range, and including only a single q (effective potential) parameter, the results are more useful. Comparison with the results of the previous analysis,[22] also given in Table 1, shows that the parameters have changed by amounts that are many times greater than the respective statistical errors. This is due to the difference between the models but also large parameter correlations, particularly between quadratic baseline function coefficients and the line profile parameters. As discussed above, the multispectrum fit used here produces statistical errors that ignore pressure measurement errors, and these statistical parameter errors are unrealistically small.

$\gamma(T_0)$ and n_γ for self-collisions are compared to the previous SDV determinations in Figure 3(a). $\gamma(T_0)$ falls outside the uncertainty of the previous value as a result of the constraints added to the fitting procedure, but the current analysis is more useful in terms of predicting profiles at different temperatures within the current range and results in a better representation of the measurements. The differences in the lower panel Figure 3(b) reflect the different models used in several of the earlier works. Figure 4a shows the individual $\delta(T)$ for each

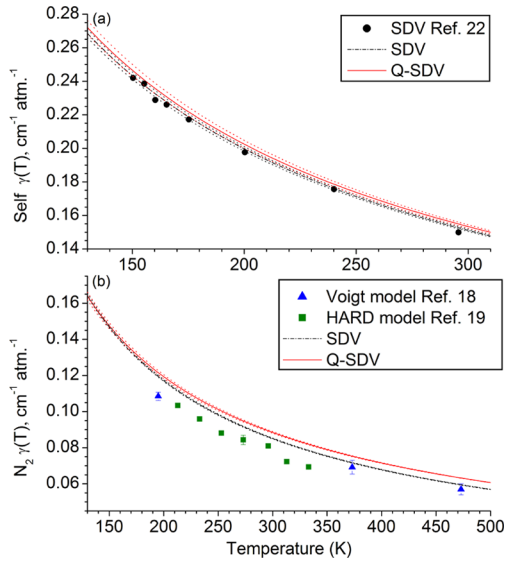

Figure 3. Temperature-dependent broadening $\gamma(T)$ for (a) self- and (b) N_2-broadened measurements with comparisons to previous studies. Line shape models used are as noted, and plotted lines are calculated from Tables 1 and 2. Dotted lines show uncertainties as one standard deviation derived from the assumption of a 0.5% pressure measurement uncertainty; see text for details. Statistical error bars are shown as one standard deviation and are in many cases smaller than the points.

dx.doi.org/10.1021/jp408960e | J. Phys. Chem. A 2013, 117, 13908−13918

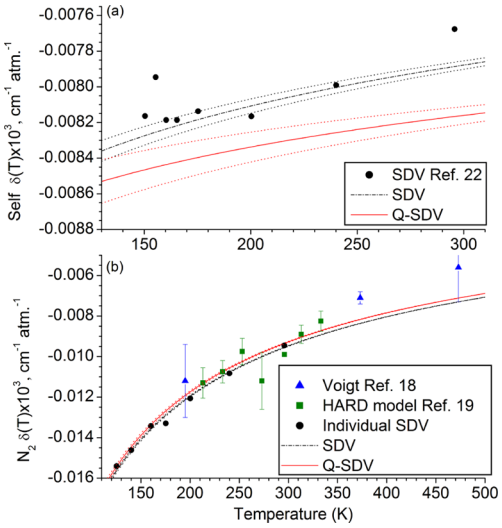

Figure 4. Temperature-dependent shift $\delta(T)$ for (a) self- and (b) N_2-broadened measurements with comparisons to previous studies. Line shape models used are as noted and plotted lines are calculated from Tables 1 and 2 with dotted lines indicating one standard deviation of the variation derived from the assumption of a 0.5% pressure uncertainty; see text for details. The points "Individual SDV" shown in panel b are from preliminary fits of the current data and were used to establish that $\delta(T)$ follows a power law for temperature dependence in the range of the present data. Statistical error bars are shown as one standard deviation, and in many cases are smaller than the points.

temperature and a comparison to the previous results. The temperature dependence is very weak for the self-collision data, but based on the observed trend in the more strongly temperature-dependent N_2 $\delta(T)$ discussed below, our final results for C_2H_2 data have been constrained to follow eq 1. The n_δ and $\delta(T_0)$ values are also reported in Table 1.

Table 2 summarizes the same results for the N_2-broadening and compares them to other analyses. In some cases, we have recomputed published values in a manner consistent with our own statistical determinations either because the authors did not report a value or adopted different analysis methods. Details are given in the table notes. The acetylene-N_2 parameters determined have similar accuracy to those found for self-collisions. Both n_γ and n_δ are larger than the respective self-collision parameters, indicating larger temperature effects on the broadening and shift for pressure broadening due to collisions with nitrogen. In the case of the shift, the strong temperature dependence seen in the points in Figure 4b allowed us to observe a clear trend that could be successfully modeled by eq 1. This allowed us to fit the temperature dependence in the multispectrum fit rather than determining a parameter at each temperature.

Data from other temperature-dependent C_2H_2–N_2 studies in this band[18,19] are included in Figures 3b and 4b. Campbell et al.[18] reported one measurement within the present data's temperature range, at 195 K, and two higher temperature measurements at 373 and 473 K. Rozario et al.[19] reported measurements at seven temperatures ranging from 213 to 333 K. In ref 18, the data were fit to a Voigt profile, and the pressure broadening parameters so derived are systematically lower than the plotted line representing $\gamma_{N2}(T_{ref})$ and $n_{\gamma,N2}$ from the current study. This is probably a result of the neglect of any narrowing in the Voigt profile, rather than any measurement inconsistency. Campbell et al. also determined a temperature exponent, n_γ, which matches the present value to within quoted uncertainties. Of the data presented in Rozario et al.,[19] we chose to compare to the hard collision model data. The temperature-dependent parameter n_γ is once again in good agreement with our value, with individual $\gamma_{N2}(T)$ values again systematically lower than ours. In ref 19, fixed narrowing parameters were used, and we speculate these may have been estimated too high (in the case of C_2H_2–C_2H_2) or too low (C_2H_2–N_2), giving rise to the differences we observe.

Figure 4b plots the data relating to the N_2 pressure shift. Data points from refs 18 and 19 show good agreement to our own within experimental uncertainty. The $\gamma_{N2}(T_{ref})$ points in ref 18 are lower than those determined here, which can likely be explained by fitting line profiles that include some narrowing contribution with a Voigt profile. Based on the similarities between the data sets, we believe eq 1 can be used successfully to extend both our broadening and shift parameters to the higher temperatures where data was measured in ref 18.

4.3. Q-SDV Modeling. Tables 1–4 and Figures 3–6 contain results obtained with the Q-SDV model. Broadening and shift parameters are very similar to those determined using the SDV model, as one would expect. An advantage of using the Q-SDV is that one can determine how the narrowing and asymmetry change with temperature, while in the frequency domain SDV with a global q, the temperature dependence is part of the assumed physical model. Figure 5 shows narrowing parameter data points, labeled "Individual Q-SDV", obtained from self- and N_2-broadened fits where only the broadening

Table 2. N_2-Broadened Line Shape Parameters for the P(11) Line of $\nu_1 + \nu_3$

	SDV		Q-SDV			
fitted parameter	value (uncertainty)	P-smeared uncertainty	value (uncertainty)	P-smeared uncertainty	ref 18[b]	ref 19[c]
$\gamma(T_0)$[a]	0.086022(13)	0.0003	0.089351(19)	0.0005	---	0.08095(95)
n_γ	0.78678(18)	0.005	0.73771(35)	0.009	0.75(3)	0.75(8)[d]
$\delta(T_0)$[a]	−0.009548(2)	0.00002	−0.00[b]9346(4)	0.00003	−0.00837(12)[d]	−0.0099(1)
n_δ	0.57323(38)	0.004	0.58295(80)	0.006	0.717(57)[d]	0.57(20)[d]
q	6.814(7)	0.03	---	---	---	---
$\gamma_2(T_0)$[a]	---	---	0.01383(2)	0.0003	---	---
$n_{\gamma 2}$	---	---	0.458(2)	0.04	---	---
$\delta_2(T)$[a]	---	---	see table 4	see table 4	---	---

[a]Units are cm^{-1}/atm. Reference temperature T_0 is 296 K. Values are reported with one standard deviation in parentheses. Columns 3 and 5: Uncertainties obtained by assuming a 0.5% pressure uncertainty, and Monte Carlo sampling; see text for details. $\delta_2(T)$ parameters can be found in Table 4 for the Q-SDV model. [b]Voigt model results. [c]Hard model results. P(11) estimate based on averaged results from P(10) and P(12) measurements. [d]Calculated using eq 1 and weighted least-squares fit to reported $\gamma_{N2}(T)$ and $\delta_{N2}(T)$ values, for comparison.

dx.doi.org/10.1021/jp408960e | J. Phys. Chem. A 2013, 117, 13908–13918

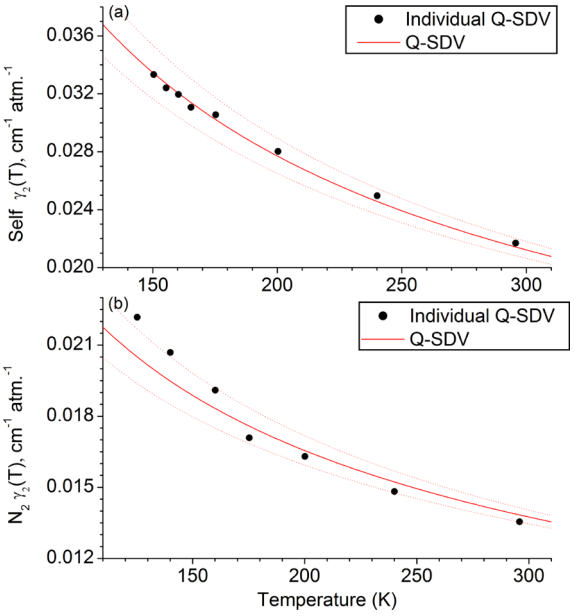

Figure 5. Temperature-dependent narrowing $\gamma_2(T)$ for (a) self- and (b)N_2-broadened measurements and the Q-SDV model. Points "Individual Q-SDV" are from Tables 3 and 4 and were used to determine that $\gamma_2(T)$ follows a power law in temperature dependence. The plotted lines were produced from the final fitted values for $\gamma_2(T_0)$ and $n_{\gamma 2}$ from Tables 1 and 2, and dotted lines show errors obtained by assuming a 0.5% pressure uncertainty; see text for details. Statistical errors of one standard deviation are smaller than the points.

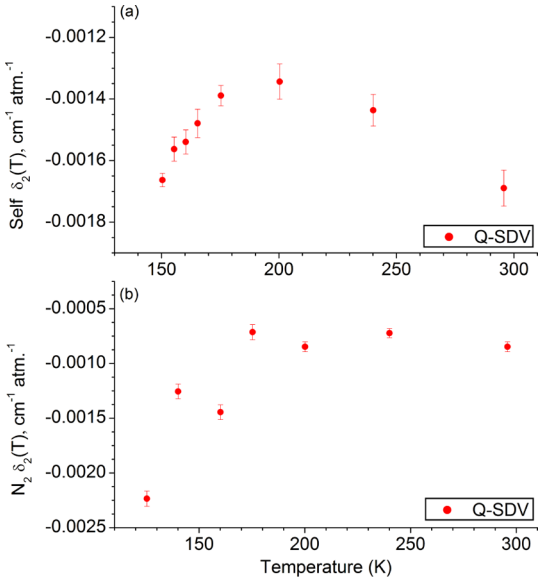

Figure 6. Temperature-dependent asymmetry $\delta_2(T)$ for (a) self- and (b)N_2-broadened measurements from the Q-SDV model. Plots were made with the final fit results from Tables 3 and 4. $\delta_2(T)$ has a clear nonpower law temperature dependence, which was not modeled. Error bars shown were obtained by assuming a 0.5% pressure uncertainty; see text for details.

$\gamma(T)$ temperature dependence was fixed to the power law, eq 1. In both cases, but for self-collisions especially, the points display a power law dependence. The temperature dependence of the speed-dependent narrowing is more difficult to measure, and we are not aware of any other reports in the literature. For models based on Dicke-type narrowing, a temperature dependence was recently reported for C_2H_2[21,60] and Ar-perturbed H_2O.[61] In these three cases, the authors also found a power law temperature dependence. If Dicke narrowing is related to the gas diffusion coefficient[62,63] a $T^{-1/2}$ temperature dependence can be predicted, so the present results are not unexpected.

A Taylor Series approximation to the speed-dependent Galatry profile[48] suggests that the value of Dicke narrowing, γ_{Dicke}, would need to be approximately 3 times that of γ_2 to give an equivalent narrowing contribution, and this has been confirmed in our work on CN radical.[50] Assuming this relationship, 3 times the value of $\gamma_{2\text{self}}$ (0.022 cm^{-1}·atm^{-1}) we determine, exactly corresponds to the γ_{Dicke} determined by Povey et al.[60] of 0.066(2) cm^{-1}·atm^{-1} at 293 K for another acetylene combination band in this region.

γ_{Dicke} may also be estimated from the mass diffusion constant D_m.[62,63] Values were calculated from ref 62 eqs 8.2−20 using Appendices I-A and I-M to obtain relevant values. Shown in Tables 3 and 4, calculated D_m values are between 1.8 and 2.3

Table 3. Narrowing and Shift Parameters Derived from Q-SDV Fits to the Self-Broadened Data

average T (K)	$\gamma_2(T)$ Q-SDV	D_m calculated	$\delta_2(T)$ Q-SDV	$\delta_2(T)$ P-smeared uncertainty
295.715(19)	0.02169(1)	0.040	−0.001689(6)	0.00006
240.135(25)	0.02495(1)	0.048	−0.001437(5)	0.00005
200.298(49)	0.02802(1)	0.057	−0.001344(5)	0.00006
175.319(16)	0.03055(1)	0.066	−0.001389(5)	0.00003
165.373(12)	0.03107(1)	0.070	−0.001479(5)	0.00005
160.343(5)	0.03195(1)	0.072	−0.001540(6)	0.00004
155.373(3)	0.03240(1)	0.074	−0.001563(7)	0.00004
150.383(20)	0.03333(1)	0.077	−0.001663(8)	0.00002

Column 2: speed-dependence of broadening, $\gamma_2(T)$, obtained from a Q-SDV model fit where only $\gamma(T)$ is constrained to the power law in eq 1. Column 3: Calculated mass diffusion constant D_m values. Column 4: Self-broadened asymmetry due to the speed dependence of shift, $\delta_2(T)$, obtained from the final Q-SDV model results in which the temperature dependence of $\gamma(T)$, $\delta(T)$, and $\gamma_2(T)$ are constrained to follow eq 1. Values have one standard deviation in parentheses, and units are cm^{-1}/atm. Column 5: Uncertainties obtained by assuming a 0.5% pressure uncertainty and Monte Carlo sampling; see text for details.

times the size of $\gamma_2(T)$ for self-broadened C_2H_2 and between 2.5 and 3.3 times the size of $\gamma_2(T)$ for N_2-broadened C_2H_2, although the sign of the temperature-dependent slope agrees in both cases. We note, however, that the temperature dependence of the calculated diffusion coefficient does not match what is inferred from the observed line narrowing. Another consistency check is afforded by examination of the temperature dependence of the broadening $[\partial\gamma(T)/\partial T]$ may be related to the speed-dependent narrowing as shown by Looney[40] eq 5.46,

$$\gamma_2(T) = 2T\left(\frac{\mu}{m_a}\right)\left(\frac{\partial\gamma(T)}{\partial T}\right) \quad (8)$$

where μ is the reduced mass of the absorber and perturber. When the equations are evaluated, for pure C_2H_2 we estimated $\gamma_2 = 0.012$ from $[\partial\gamma(T)/\partial T]$, while the fitted result (Table 1) is 0.022, both in cm^{-1} atm^{-1} units. The result is similar for the nitrogen-broadened terms, with the value estimated from the T-

dx.doi.org/10.1021/jp408960e | J. Phys. Chem. A 2013, 117, 13908−13918

Table 4. Narrowing and Shift Parameters Derived from Q-SDV Fits to the N_2-Broadened Data

average T (K)	$\gamma_2(T)$ Q-SDV	D_m calculated	$\delta_2(T)$ Q-SDV	$\delta_2(T)$ P-smeared uncertainty
295.851(19)	0.01355(2)	0.031	−0.000600(7)	0.00005
240.080(20)	0.01482(1)	0.037	−0.000412(6)	0.00004
200.145(71)	0.01630(1)	0.044	−0.000626(6)	0.00005
175.281(96)	0.01709(1)	0.050	−0.000737(9)	0.00007
160.128(33)	0.01910(5)	0.054	−0.001382(24)	0.00007
140.117(44)	0.02069(2)	0.061	−0.001262(13)	0.00007
125.300(2)	0.02218(3)	0.069	−0.002307(17)	0.00007

Column 2: speed-dependence of broadening, $\gamma_2(T)$, obtained from a Q-SDV model fit where only $\gamma(T)$ is constrained to the power law in eq 1. Column 3: Calculated mass diffusion constant D_m values. Column 4: N_2-broadened asymmetry due to the speed dependence of shift, $\delta_2(T)$, obtained from the final Q-SDV model results in which $\gamma(T)$, $\delta(T)$, and $\gamma_2(T)$ are constrained to eq 1 for temperature dependence. Values have one standard deviation in parentheses, and units are cm^{-1}/atm. Column 5: Uncertainties obtained by assuming a 0.5% pressure uncertainty and Monte Carlo sampling; see text for details.

dependence of $\gamma(T)$, approximately one-half of the fitted narrowing value in Table 2.

It could be argued that we are modeling combined contributions to the line shape from Dicke and speed-dependent narrowing[39,42] with a single effective (speed-dependent) effect here. Physically, the Dicke narrowing should change the shape of the speed distribution in our gas, while speed-dependent narrowing is a result of slower moving molecules (near the line center) having fewer collisions. To investigate this, attempts were made to fix Dicke narrowing to the values derived from D_m, or scaled values that took into account the higher collision rates assumed in a soft collision model, but this did not improve the line shape fits; the parameters in the speed-dependent Galatry profile are completely correlated given our data. Our analysis was not limited to strictly positive values for the narrowing mechanisms. It is possible that further measurements would permit the simultaneous determination of these closely related parameters. In our final determination, the temperature dependence of the speed-dependent narrowing parameter was constrained to a power law, and the $\gamma_2(T_0)$ and $n_{\gamma 2}$ were fit and are given in Tables 1 and 2. The results from the individual Q-SDV fits were included in Tables 3 and 4.

Values for the speed-dependent shift parameter (δ_2) as a function of temperature plots are shown in Figure 6. These plots come from the final Q-SDV fit which uses the power law from eq 1 for the temperature dependence of the broadening, shifting, and narrowing. This is one of the first times that asymmetry parameters have been measured for acetylene line profiles, and there are no precedents to compare to this. We note a very clear trend, but we are hesitant to fit it to a function since the power law behavior seen in the other parameters is absent here. However, $\delta_2(T)$ points here can be used to get a very good estimate of $\delta_2(T)$ at other temperatures within the studied range using interpolation. The physical reason for the curve is unknown, but it is possible that not all the asymmetry comes from the speed-dependent shift. Other studies have modeled asymmetry using Dicke narrowing[40,63] and an assumed correlation between velocity changing and dephasing processes. Typical data as referred to in Figure 2 shows the Q-SDV does effectively model the small observed line asymmetry in the current system. However, it is not clear why; in the case of self-broadening, $\delta(T)$ has a weak temperature dependence, while $\delta_2(T)$ shows such a pronounced change with temperature.

5. CONCLUSIONS

From data obtained using a frequency comb-stabilized extended cavity diode laser, parameters for the self- and N_2-broadened line shape for the P(11) transition in the $\nu_1 + \nu_3$ band of acetylene have been determined to high accuracy. The results will be useful in the analysis of pressure-broadened spectra in various environments and determine accurate pressure-dependent broadening and shift parameters for comparison to theory. The analyses also reinforce the strengths and weaknesses of a multispectrum analysis that fits all temperatures and pressures simultaneously with a reduced set of parameters, but requires a more careful assessment of the error propagation. The SDV and Q-SDV model fits are very close to the noise level of the current experiment, but it is important to continue to test different types of models to assess their strengths and weaknesses as there are still small systematic differences between the observed and calculated line shapes. For the current work, however, observed asymmetry is small and either the SDV or Q-SDV models provide very good results. The multispectrum fit results in unrealistically small statistical uncertainties for line shape parameters when frequencies are highly accurate and pressure errors dominate the measurements. A more sensible estimate and upper limit was calculated using Monte Carlo methods to account for pressure uncertainties.

We have a preference for the Q-SDV model expressed, as it is here, in the time domain, as the resulting parameters are not dependent on approximations in a physically unrealistic model. The relaxation parameters in the Q-SDV, and the extended Q-SDV model, are model-dependent only to the extent that the quadratic form has been assumed to describe the absorber speed dependence of the relaxation rate after collision with a partner with a Boltzmann distribution of speeds. These quantities can, in principle, be calculated from first principles using realistic intermolecular potentials and compared to the experimental results.

Future work will extend the present measurements to include higher concentration mixtures, multiple rotational transitions, and overlapped lines to quantify line-mixing for other acetylene lines in the 1.5 μm region.

AUTHOR INFORMATION

Corresponding Author

*E-mail: Sears@bnl.gov.

Author Contributions

‡The manuscript was written through contributions of all authors. All authors have given approval to the final version of the manuscript. These authors contributed equally.

Notes

The authors declare no competing financial interest.

ACKNOWLEDGMENTS

Acknowledgement is made to the Donors of the American Chemical Society Petroleum Research Fund for partial support of this research. We are grateful for Program Development Funding awarded to T.J.S. by Brookhaven National Laboratory,

which provided funds for some of the equipment used in this work. A.W.M. gratefully acknowledges support by NASA EPSCoR Grant No. PS 4990 for supporting the development of low temperature cells. Work at Brookhaven National Laboratory was carried out under Contract No. DE-AC02-98CH10886 with the U.S. Department of Energy, Office of Science, and supported by its Division of Chemical Sciences, Geosciences and Biosciences within the Office of Basic Energy Sciences.

REFERENCES

(1) Varanasi, P.; Bangaru, R. P. Intensity and half-width measurements in the 1.525 μm band of acetylene. *J. Quant. Spectrosc. Radiat. Transfer* **1975**, *15*, 267−273.

(2) Minutolo, P.; Corsi, C.; D'Amato, F.; DeRosa, M. Self- and foreign broadening and shift coefficients for C_2H_2 lines at 1.54 μm. *Eur. Phys. J. D* **2001**, *17*, 175−179.

(3) Gilbert, S. L.; Swann, W. C. 'Acetylene $^{12}C_2H_2$ absorption reference for 1510 to 1540 nm wavelength calibration—SRM 2517a. *NIST special publication* **2001**, *260*, 133.

(4) Rudolph, J.; Ehhalt, D. H.; Khedim, A. Vertical Profiles of Acetylene in the Troposphere and Stratosphere. *J. Atmos. Chem.* **1984**, *2* (2), 117−124.

(5) Zander, R.; Rinsland, C. P.; Ehhalt, D. H.; Rudolph, J.; Demoulin, P. Vertical Column Abundances and Seasonal Cycle of Acetylene, C_2H_2, above the Jungfraujoch Station, Derived from IR Solar Observations. *J. Atmos. Chem.* **1991**, *13* (4), 359−372.

(6) Goldman, A.; Murcray, F.; Blatherwick, R.; Gillis, J.; Bonomo, F.; Murcray, F.; Murcray, D.; Cicerone, R. Identification of acetylene (C_2H_2) in infrared atmospheric absorption spectra. *J. Geophys. Res.* **1981**, *86* (C12), 12143−12146.

(7) Kanakidou, M.; Bonsang, B.; Le Roulley, J.; Lambert, G.; Martin, D.; Sennequier, G. Marine source of atmospheric acetylene. *Nature* **1988**, 333 (6168), 51−52.

(8) Oremland, R. S.; Voytek, M. A. Acetylene as fast food: Implications for development of life on anoxic primordial Earth and in the outer solar system. *Astrobiology* **2008**, *8* (1), 45−58.

(9) Coustenis, A. Formation and evolution of Titan's atmosphere. *Space Sci. Rev.* **2005**, *116* (1−2), 171−184.

(10) Didriche, K.; Herman, M. A four-atom molecule at the forefront of spectroscopy, intramolecular dynamics and astrochemistry: Acetylene. *Chem. Phys. Lett.* **2010**, *496* (1), 1−7.

(11) De Labachelerie, M.; Nakagawa, K.; Ohtsu, M. Ultranarrow $^{13}C_2H_2$ saturated-absorption lines at 1.5 μm. *Opt. Lett.* **1994**, *19* (11), 840−842.

(12) Nakagawa, K.; De Labachelerie, M.; Awaji, Y.; Kourogi, M. Accurate optical frequency atlas of the 1.5-μm bands of acetylene. *J. Opt. Soc. Am. B* **1996**, *13* (12), 2708−2714.

(13) Edwards, C. S.; Margolis, H. S.; Barwood, G. P.; Lea, S. N.; Gill, P.; Huang, G.; Rowley, W. R. C. Absolute frequency measurement of a 1.5-μm acetylene standard by use of a combined frequency chain and femtosecond comb. *Opt. Lett.* **2004**, *29* (6), 566−568.

(14) Madej, A. A.; Alcock, A. J.; Czajkowski, A.; Bernard, J. E.; Chepurov, S. Accurate absolute reference frequencies from 1511 to 1545 nm of the $\nu_1 + \nu_3$ band of $^{12}C_2H_2$ determined with laser frequency comb interval measurements. *J. Opt. Soc. Am. B* **2006**, *23*, 2200−2208.

(15) Edwards, C. S.; Barwood, G. P.; Margolis, H. S.; Gill, P.; Rowley, W. R. C. High-precision frequency measurements of the $\nu_1 + \nu_3$ combination band of $(C_2H_2)-^{12}C$ in the 1.5 μm region. *J. Mol. Spectrosc.* **2005**, *234* (1), 143−148.

(16) Edwards, C. S.; Margolis, H. S.; Barwood, G. P.; Lea, S. N.; Gill, P.; Rowley, W. R. C. High-accuracy frequency atlas of $^{13}C_2H_2$ in the 1.5 μm region. *Appl. Phys. B: Laser Opt.* **2005**, *80*, 977−983.

(17) Arteaga, S. W.; Bejger, C. M.; Gerecke, J. L.; Hardwick, J. L.; Martin, Z. T.; Mayo, J.; McIlhattan, E. A.; Moreau, J.-M. F.; Pilkenton, M. J.; Polston, M. J.; et al. Line broadening and shift coefficients of acetylene at 1550 nm. *J. Mol. Spectrosc.* **2007**, *243*, 253−266.

(18) Campbell, N. T.; Cook, J. D.; Coombs, B. A.; Fuller, E. P.; Hardwick, J. L.; Hurley, S. M.; Ho, L. K.; Kovac, P. A.; Robertson, E. J.; Senning, E. N.; et al. Temperature dependence of pressure broadening and shifts of acetylene at 1550 nm by N_2. *Mol. Phys.* **2011**, *109* (17−18), 2199−2208.

(19) Rozario, H.; Garber, J.; Povey, C.; Hurtmans, D.; Buldyreva, J.; Predoi-Cross, A. Experimental and theoretical study of N_2-broadened acetylene line parameters in the $\nu_1 + \nu_3$ band over a range of temperatures. *Mol. Phys.* **2012**, *110* (21−22), 2645−2663.

(20) Bond, K. S.; Collett, N. D.; Hardwick, J. L.; Hinds, E. E.; Keiber, T. W.; Kelly-Morgan, I. S. G.; Matthys, C. M.; Pilkenton, M. J.; Sinclair, K. W.; Taylor, A. A. Temperature dependence of pressure broadening and shifts of acetylene at 1550 nm by He, Ne and Ar. *Appl. Phys. B: Laser Opt.* **2008**, *90*, 255−262.

(21) Povey, C.; Guillorel-Obregon, M.; Predoi-Cross, A.; Ivanov, S. V.; Buzykin, O. G.; Thibault, F. Low pressure line shape study of nitrogen perturbed acetylene transitions in the $\nu_1+ \nu_3$ band over a range of temperatures. *Can. J. Phys.* **2013**, DOI: 10.1139/cjp-2013-0031.

(22) Cich, M.; McRaven, C.; Lopez, G.; Sears, T.; Hurtmans, D.; Mantz, A. Temperature-dependent pressure broadened line shape measurements in the $\nu_1+ \nu_3$ band of acetylene using a diode laser referenced to a frequency comb. *Appl. Phys. B: Lasers Opt.* **2012**, *109*, 373−384.

(23) Margolis, H. S. Spectroscopic applications of femtosecond optical frequency combs. *Chem. Soc. Rev.* **2012**, *41*, 5174−5184.

(24) McRaven, C. P.; Cich, M. J.; Lopez, G. V.; Sears, T. J.; Hurtmans, D.; Mantz, A. W. Frequency comb-referenced measurements of self- and nitrogen- broadening in the $\nu_1 + \nu_3$ band of acetylene. *J. Mol. Spectrosc.* **2011**, *266* (1), 43−51.

(25) Gambetta, A.; Gatti, D.; Castrillo, A.; Coluccelli, N.; Galzerano, G.; Laporta, P.; Gianfrani, L.; Marangoni, M. Comb-assisted spectroscopy of CO_2 absorption profiles in the near-and mid-infrared regions. *Appl. Phys. B: Lasers Opt.* **2012**, 1−6.

(26) Long, D. A.; Truong, G.-W.; Zee, R. V.; Plusquellic, D. F.; Hodges, J. T. Cavity-enhanced, frequency-agile rapid scanning (FARS) spectroscopy: experimental realizations and measurement results. 68th Ohio State University International Symposium on Molecular Spectroscopy, Columbus, OH, 2013.

(27) Ward, J.; Cooper, J.; Smith, E. W. Correlation Effects in Theory of Combined Doppler and Pressure Broadening 0.1. Classical Theory. *J. Quant. Spectrosc. Radiat. Transfer* **1974**, *14* (7), 555−590.

(28) Hartmann, J. M.; Boulet, C.; Robert, D. *Collisional Effects on Molecular Spectra*, 1st ed.; Elsevier: Amsterdam, 2008; p 411.

(29) Rautian, S. G.; Sobel'man, I. I. The effect of collisions on the Doppler broadening of spectral lines. *Sov. Phys. Uspekhi* **1967**, *9*, 701−716.

(30) Lance, B.; Blanquet, G.; Walrand, J.; Bouanich, J. P. On the speed-dependent hard collision lineshape models: Application to C_2H_2 perturbed by Xe. *J. Mol. Spectrosc.* **1997**, *185* (2), 262−271.

(31) Galatry, L. Simultaneous effect of Doppler and foreign gas broadening on spectral lines. *Phys. Rev. Lett.* **1961**, *122*, 1218−1223.

(32) Hurtmans, D.; Dufour, G.; Bell, W.; Henry, A.; Valentin, A.; Camy-Peyret, C. Line intensity of R(0) and R(3) of the $^{12}CH_4$ $2\nu_3$ band from diode laser spectroscopy. *J. Mol. Spectrosc.* **2002**, *215*, 128−133.

(33) Benner, D. C.; Rinsland, C. P.; Devi, V. M.; Smith, M. A. H.; Atkins, D. A multispectrum nonlinear least squares fitting technique. *J. Quant. Spectrosc. Radiat. Transfer* **1995**, *53* (6), 705−721.

(34) Mantz, A. W.; Malathy-Devi, V.; Benner, D. C.; Smith, M. A. H.; Peredoi-Cross, A.; Dulick, M. A multispectrum analysis of widths and shifts in the 2010−2260 region of $^{12}C^{16}O$ broadened by helium at temperatures between 80 and 297 K. *J. Molec. Struct.* **2005**, *742*, 99−100.

(35) Tickner, A.; Lossing, F. The Measurement of Low Vapor Pressures by Means of a Mass Spectrometer. *J. Phys. Chem.* **1951**, *55* (5), 733−740.

(36) Li, J. S.; Durry, G.; Cousin, J.; Joly, L.; Parvitte, B.; Zeninari, V. Self-broadening coefficients and positions of acetylene around 1.533

μm studied by high resolution diode laser absorption spectroscopy. *J. Quant. Spectrosc. Radiat. Transfer* **2010**, *111*, 2332−2340.
(37) Farrow, R. L.; Rahn, L. A.; Sitz, G. O.; Rosasco, G. J. Observation of a speed dependent collisional inhomogeneity in H_2 line profiles. *Phys. Rev. Lett.* **1989**, *63*, 746−749.
(38) Lisak, D.; Rusciano, G.; Sasso, A. An accurate comparison of lineshape models on H_2O lines in the spectral region around 3 μm. *J. Mol. Spectrosc.* **2004**, *227* (2), 162−171.
(39) Lisak, D.; Rusciano, G.; Sasso, A. Speed-dependent and correlation effects on the line shape of acetylene. *Phys. Rev. A* **2005**, *72* (1), 012503.
(40) Looney, J. P. Comprehensive Theory for the Broadening, Shifting and Narrowing of HF and HCI Fundamental Band Absorption Profiles. Ph.D. Thesis, Pennsylvania State University, 1987.
(41) Duggan, P.; Sinclair, P. M.; May, A. D.; Drummond, J. R. Line-Shape Analysis of Speed-Dependent Collisional Width Inhomogeneities in CO Broadened by Xe, N_2, and He. *Phys. Rev. A* **1995**, *51* (1), 218−224.
(42) Duggan, P.; Sinclair, P.; Berman, R.; May, A.; Drummond, J. R. Testing Lineshape Models: Measurements for ν = 1−0 CO Broadened by He and Ar. *J. Mol. Spectrosc.* **1997**, *186* (1), 90−98.
(43) Rosenkranz, P. W. Shape of 5 mm Oxygen Band in Atmosphere. *IEEE Trans. Antennas Propagation* **1975**, *AP23* (4), 498−506.
(44) Rothman, L. S.; Gordon, I. E.; Babikov, Y.; Barbe, A.; Chris Benner, D.; Bernath, P. F.; Birk, M.; Bizzocchi, L.; Boudon, V.; Brown, L. R.; et al. The HITRAN2012 molecular spectroscopic database. *J. Quant. Spectrosc. Radiat. Transfer* **2013**, *130* (0), 4−50.
(45) Povey, C.; Predoi-Cross, A.; Hurtmans, D. R. Line shape study of acetylene transitions in the $\nu_1 + \nu_2 + \nu_4 + \nu_5$ band over a range of temperatures. *J. Mol. Spectrosc.* **2011**, *268* (1−2), 177−188.
(46) Bouanich, J. P.; Predoi-Cross, A. Theoretical calculations for line-broadening and pressure-shifting in the $\nu_1 + \nu_2 + \nu_4 + \nu_5$ band of acetylene over a range of temperatures. *Mol. Phys.* **2011**, *109* (17−18), 2071−2081.
(47) Ciuryło, R.; Szudy, J. Speed-dependent pressure broadening and shift in the soft collision approximation. *J. Quant. Spectrosc. Radiat. Transfer* **1997**, *57* (3), 411−423.
(48) Priem, D.; Rohart, F.; Colmont, J.-M.; Wlodarczak, G.; Bouanich, J.-P. Lineshape study of the $J = 3 \leftarrow 2$ rotational transition of CO perturbed by N_2 and O_2. *J. Mol. Struct.* **2000**, *517*, 435−454.
(49) D'Eu, J. F.; Lemoine, B.; Rohart, F. Infrared HCN lineshapes as a test of Galatry and speed-dependent Voigt profiles. *J. Mol. Spectrosc.* **2002**, *212* (1), 96−110.
(50) Forthomme, D.; McRaven, C. P.; Sears, T. J.; Hall, G. E. Argon-Induced Pressure Broadening, Shifting and Narrowing in the CN $A^2\Pi - X^2\Sigma^+(1-0)$ Band. *J. Phys. Chem. A* **2013**, x DOI: 10.1021/jp4030359.
(51) Henry, A.; Hurtmans, D.; Margottin Maclou, M.; Valentin, A. Confinement narrowing and absorber speed dependent broadening effects on CO lines in the fundamental band perturbed by Xe, Ar, Ne, He and N_2. *J. Quant. Spectrosc. Radiat. Transfer* **1996**, *56* (5), 647−671.
(52) Brault, J.; Brown, L.; Chackerian, C., Jr.; Freedman, R.; Predoi-Cross, A.; Pine, A. Self-broadened $^{12}C^{16}O$ line shapes in the $\nu = 2 \leftarrow 0$ band. *J. Mol. Spectrosc.* **2003**, *222* (2), 220−239.
(53) Pine, A.; Markov, V. Self-and foreign-gas-broadened lineshapes in the ν_1 band of NH_3. *J. Mol. Spectrosc.* **2004**, *228* (1), 121−142.
(54) Boone, C. D.; Walker, K. A.; Bernath, P. F. An efficient analytical approach for calculating line mixing in atmospheric remote sensing applications. *J. Quant. Spectrosc. Radiat. Transfer* **2011**, *112* (6), 980−989.
(55) Koshelev, M. A.; Tretyakov, M. Y.; Rohart, F.; Bouanich, J.-P. Speed dependence of collisional relaxation in ground vibrational state of OCS: Rotational behaviour. *J. Chem. Phys.* **2012**, *136*, 124316.
(56) El Hachtouki, R.; Vander Auwera, J. Absolute line intensities in acetylene. The 1.5 μm region. *J. Mol. Spectrosc.* **2002**, *216* (2), 355−362.
(57) Bottomley, G.; Reeves, C.; Seiflow, G. *P-V-T* properties of acetylene. *J. Appl. Chem.* **1959**, *9* (10), 517−518.
(58) Gamache, R. R.; Arié, E.; Boursier, C.; Hartmann, J.-M. Pressure-broadening and pressure-shifting of spectral lines of ozone. *Spectrochim. Acta, Part A: Mol. Biomol. Spectrosc.* **1998**, *54* (1), 35−63.
(59) Bevington, P. R.; Robinson, D. K. *Data Reduction and Error Analysis for the Physical Sciences*, 3rd ed.; McGraw-Hill: New York, 2003; p 319.
(60) Povey, C.; Predoi-Cross, A.; Hurtmans, D. R. Low-pressure line shape study of acetylene transitions in the $\nu_1 + \nu_2 + \nu_4 + \nu_5$ band over a range of temperatures. *Mol. Phys.* **2012**, *110* (21−22), 2633−2644.
(61) Li, H.; Farooq, A.; Jeffries, J. B.; Hanson, R. K. Diode laser measurements of temperature-dependent collisional-narrowing and broadening parameters of Ar-perturbed H_2O transitions at 1391.7 and 1397.8 nm. *J. Quant. Spectrosc. Radiat. Transfer* **2008**, *109* (1), 132−143.
(62) Hirschfelder, J. O.; Curtiss, C. F.; Bird, R. B. *Molecular Theory of Gases and Liquids*; Wiley: New York, 1954; Vol. *26*.
(63) Pine, A. Line shape asymmetries in Ar-broadened HF (ν = 1−0) in the Dicke-narrowing regime. *J. Chem. Phys.* **1994**, *101*, 3444.